PAPER

Check for updates

Iodonium salts as efficient iodine(III)-based noncovalent organocatalysts for Knorr-type reactions†

Sevilya N. Yunusova,[a] Alexander S. Novikov, [ID][a] Natalia S. Soldatova,[a] Mikhail A. Vovk [ID][b] and Dmitrii S. Bolotin [ID] *[a]

Hypervalent iodine(III)-derivatives display higher catalytic activity than other aliphatic and aromatic iodine(I)– or bromine(I)-containing substrates for a Knorr-type reaction of *N*-acetyl hydrazides with acetyl acetone to give *N*-acyl pyrazoles. The highest activity was observed for dibenziodolium triflate, for which 10 mol% resulted in the generation of *N*-acyl pyrazole from acyl hydrazide and acetyl acetone typically at 50 °C for 3.5–6 h with up to 99% isolated yields. ¹H NMR titration data and DFT calculations indicate that the catalytic activity of the iodine(III) is caused by the binding with a ketone.
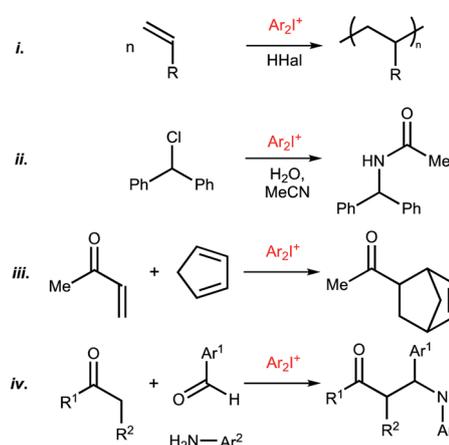
Introduction

In the past decade, organocatalysis has been the focus of extensive studies owing to its significant advantages over catalysis by metal-containing species including lower toxicity, reduced environmental footprint, and low to negligible sensitivity to air and moisture.[1,2] In general, these organocatalysts can function either through a covalent or noncovalent bonding activation. A covalent activation mode involves the formation of covalent bond(s) between a substrate and catalyst (such as amines,[1–5] heterocyclic carbenes,[1,6,7] or phosphines[8]), whereas a noncovalent mode involves the activation of substrates through noncovalent linkages to the catalyst.[2,9–18]

For noncovalent catalysis, an organic catalyst typically interacts with a substrate through hydrogen bonding (HB), and many important results were achieved for the reactions based on such HB donors as ureas,[2,19–24] squaramides,[24–26] and other Brønsted acids,[27–31] whereas catalytic reactions involving halogen (XB)[9,10,15,32–35] or chalcogen bonding (ChB)[34,36,37] are far less explored. Although XB has been established as a valuable tool in solid-state chemistry and crystal engineering,[38–41] over the last five years XB has been studied in solution[33–35,42–44] and applied to homogeneous catalytic transformations.[9,15,16,34,37]

Recently Huber and coworkers reported that iodine(III) derivatives such as diaryliodonium salts can serve as efficient organocatalysts and utilize XBs for which the catalytic activity is similar or even higher than other well-proven organocatalysts

that are based on iodine(I) derivatives, such as oligodentate 2-iodoimidazolium species.[45,46] Indeed, diaryliodonium salts exhibited a high catalytic activity in reactions in which a halide abstraction occurred[46] (including their application in living cationic polymerization of olefins;[47] Fig. 1(i) and (ii)) and in the synthetic transformations of carbonyl compounds, namely
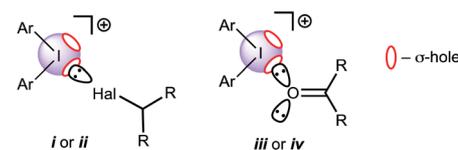

Fig. 1 Previously studied reactions catalyzed by diaryliodonium salts and plausible modes of activation of substrates. σ-hole is a region of positive electrostatic potential on an atom.[49]

aInstitute of Chemistry, Saint Petersburg State University, Universitetskaya Nab. 7/9, Saint Petersburg, 199034, Russian Federation. E-mail: d.s.bolotin@spbu.ru

bCenter for Magnetic Resonance, Saint Petersburg State University, Universitetskii Pr., 26, Saint Petersburg, 198504, Russian Federation

Diels–Alder cycloaddition[46] (Fig. 1(iii)) and Mannich reaction[48] (Fig. 1(iv)).

Considering the promising catalytic properties of diaryliodonium salts and the small number of reported examples for their application in homogeneous organocatalysis, further studies are worthwhile. In this study, we report on the catalytic activity of a series of diaryliodonium salts and provide a comparison of their activity with other XB donors in a model reaction that requires carbonyl activation. In agreement with previous suggestions that the catalytic activity of diaryliodonium salts is caused by the electrophilic activation of the electrophile,[46,47] their catalytic activity in the studied Knorr-type cyclization is caused by binding with a ketone.

Results and discussion

Knorr-type syntheses[50,51] conventionally proceed under mild conditions even in the absence of a catalyst if amines and carbonyl compounds are employed as the reactants.[52] However, for less nucleophilic hydrazine derivatives, *e.g.* 2-pyridine hydrazines[50] or acyl hydrazides,[53,54] a catalyst is desirable to conduct the reaction under mild conditions. Thus, the reaction of *N*-acyl hydrazides with 1,3-dicarbonyl compounds, which leads to *N*-acyl pyrazoles, typically requires an additional activation and is usually conducted in the presence of a Brønsted or a Lewis acid under reflux for several hours.[55–57] This reaction was chosen as a model to verify the catalytic effect of diaryliodonium salts.

Comparison of the catalytic activity for the halogen-containing organic species

Benzoyl hydrazide (**BH**) was treated with acetyl acetone (**AA**) in CD₃OD (50 °C, 5 h), which led to only a trace amount of the corresponding *N*-benzoyl pyrazole **1** (Fig. 2 and Table 1, entry 1). The addition of 1 equivalent (equiv.) of iodine(I)- or bromine(I)-containing species **A–E**, which feature expressed σ-holes at their halogen atoms,[58–60] resulted in negligible or no catalytic effect (entries 1–6). In contrast, the utilization of the dibenziodolium species **F**, **G**, and **H** led to a significant acceleration and a half-conversion was achieved after approximately 70 min (entries 7–9). Notably, other types of iodine(III) species (**I** and **J**) appeared to be catalytically inactive in the model reaction (entries 10–11) and the results obtained for the activity of **F–I** are fully consistent with the recently reported relative Lewis acidity of the iodine(III)-based XB donors.[61]

Having examined dibenziodolium triflate **H**, whose catalytic activity was the highest among all the studied halogen-containing species, we further optimized the reaction conditions. Based upon ¹H NMR monitoring of the reaction performed with various relative quantities of **AA**, we found that the optimal quantity of the carbonyl reactant was 1.2 equiv. (Fig. 3; Table 1, entries 9, 12, 13).

The S-shape of the kinetic curves was caused by the initial accumulation of the intermediate MeC(=NNHBz)CH₂COMe in the reaction mixture, which was then transformed to **1**. The overlap of the proton resonances of MeC(=NNHBz)CH₂COMe with those of the reactants and with the signals of **1** did not
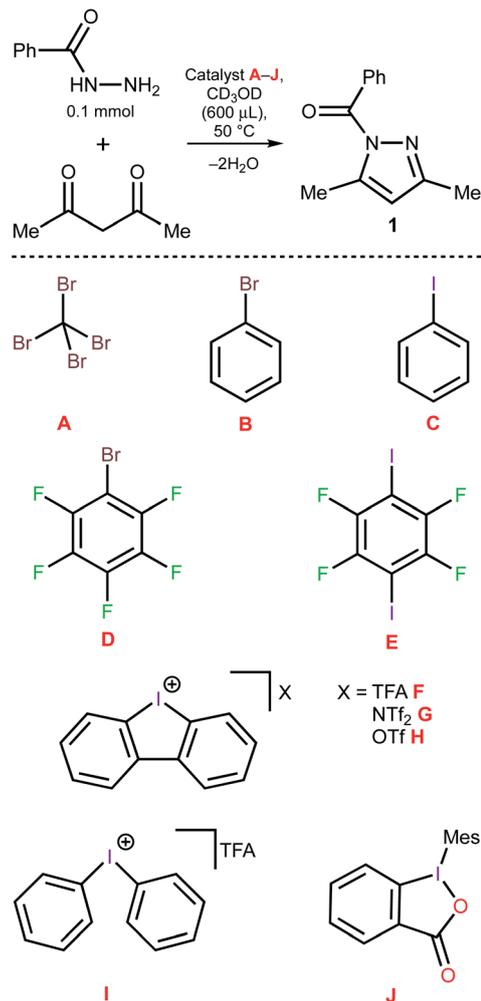

Fig. 2 Halogen-containing species tested as organocatalysts.

Table 1 Comparison of the catalytic activity of various halogen-containing species

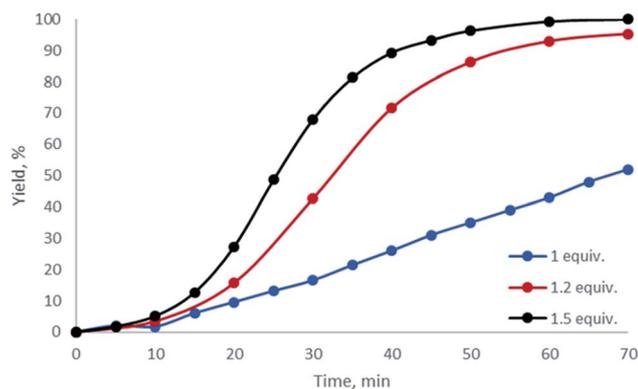| Entry	Catalyst	Catalyst load (mol%)	**AA** load (equiv.)	t (min)	Yield (%)
1	None	—	1	300	Traces
2	**A**	100	1	300	32
3	**B**	100	1	300	Traces
4	**C**	100	1	300	Traces
5	**D**	100	1	300	30
6	**E**	100	1	300	29
7	**F**	100	1	70	50
8	**G**	100	1	70	46
9	**H**	**100**	**1**	**70**	**52**
10	**I**	100	1	70	3
11	**J**	100	1	70	Traces
12	**H**	100	1.5	70	98
13	**H**	100	1.2	70	95
14	**H**	50	1.2	100	98
15	**H**	10	1.2	220	98

Fig. 3 ^{1}H NMR monitoring of the reaction of benzoyl hydrazide with various amounts of acetylacetone in the presence of 1 equiv. **H** in CD$_3$OD at 50 °C (entries 9, 12, 13). NMR yield of **1** is given on the *y*-axis.

allow the accurate calculation of its relative concentration; therefore, the corresponding plot is not provided.

Next, the relative quantity of organocatalyst **H** was varied (Fig. 4, Table 1, entries 1, 9, 14, 15) and we found that even 10 mol% of **H** effectively catalyzed the reaction and **1** could be obtained within 1 d (Table 1, entry 15).

The optimal conditions for the studied reaction were 10 mol% of **H**, 1.2 equiv. of the 1,3-dicarbonyl component, and 50 °C. Under these conditions the substrate scope was verified.

Binding of H with the reaction substrates

(i)^{1}H NMR titration. To confirm the binding of **H** with the reactants, we performed a ^{1}H NMR titration. In these experiments, **BH** or **AA** (2, 4, 6, 8, or 10 equiv.) were added to 1 equiv. of **H** in a CD$_3$CN solution (0.038 M). The titration by **BH** (Fig. 5) indicated a high-field shift (approx. 0.5 ppm) of the 2-, 3-, and 4-H resonances, whereas the 1-H resonances of H atoms located in close proximity to the I atom indicated a low-field shift by approximately 0.5 ppm (Fig. 6). Based upon the changes in the chemical shift of the 1-H protons, the **H·BH** binding constant was estimated as 2.8(2) L mol^{-1}. The opposite shift of the 1-H protons might indicate the binding of **H** with benzyl hydrazide in solution through XB as this would allow the ligated
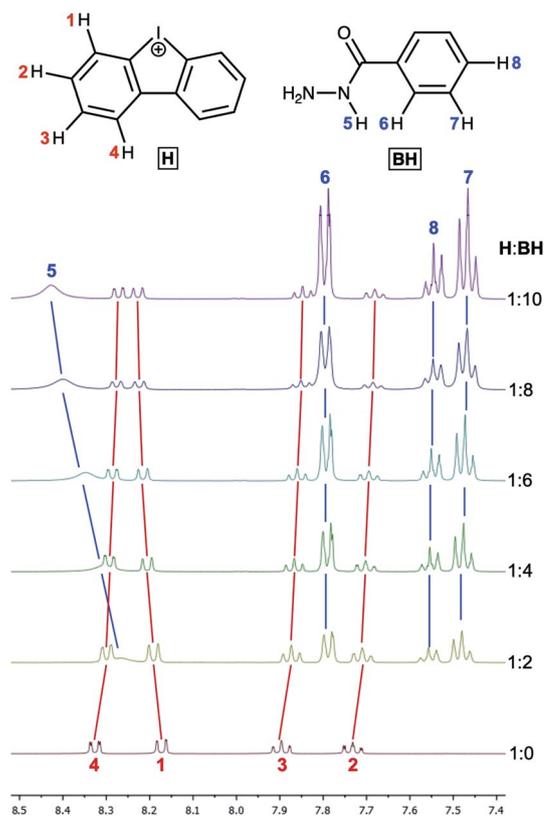

Fig. 5 The ^{1}H NMR titration of **H** by benzoyl hydrazide.

nucleophile to directly interact with the atoms while the other H atoms remain intact.

The titration of **H** by **AA** resulted in negligible changes in the chemical shifts (within 0.002 ppm) for the dibenziodolium cation, even with an excess of **AA** up to 25-fold; therefore, the corresponding binding constant could not be estimated. This observation might indicate either a low value of the binding constant or similar chemical shifts of the H atoms in the **H–AA** complex and separated substrates **H** and **AA**.

(ii) DFT calculations. Based on the ^{1}H NMR titration data, we performed DFT calculations to clarify the binding of **H** with **BH** and **AA** in a MeOH solution. Initial calculations indicated that
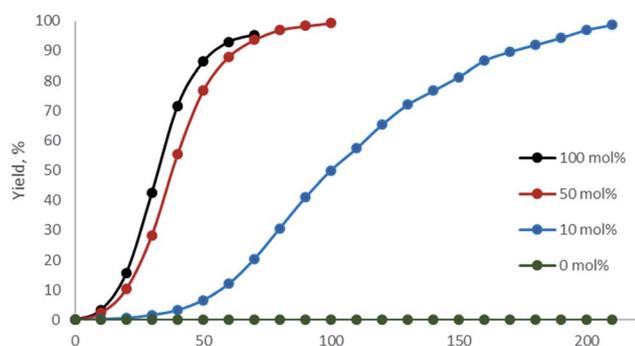

Fig. 4 ^{1}H NMR monitoring of the reaction of benzoyl hydrazide with acetylacetone with variable amount of **H** (CD$_3$OD, 50 °C; entries 1, 9, 14, 15).
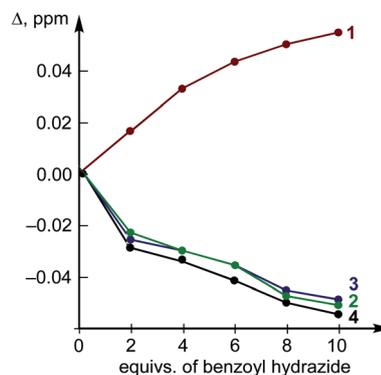

Fig. 6 The changes in chemical shifts of the **H** proton resonances upon the titration.

Table 2 The calculated Gibbs free energy (ΔG) and enthalpy change (ΔH) for direct binding of **H** with the substrates in MeOH solution[a]

Entry	Reaction	ΔG (kJ mol^{-1})	ΔH (kJ mol^{-1})
1	**H** + **BH** → **H·BH** (binding by O)	25.5	−20.9
2	**H** + **BH** → **H·BH** (binding by N)	24.7	−25.1
3	**H** + **AA** → **H·AA**	28.0	−27.2
4	i	−1.3	23.8
5	ii	1.7	22.2
6	iii	1.3	18.0

[a] **H** – dibenziodolium triflate; **BH** – benzoyl hydrazide; **AA** – acetyl acetone.

the direct coupling of the reagents is thermodynamically unfavorable in terms of the Gibbs free energy, which conflicts with the experimentally observed titration data at least for **BH** (Table 2, entries 1–3).

Considering that the enthalpies of all the reactions are negative, these results indicate the significant impact of entropy change in the model systems. Accordingly, we included MeOH solvent molecules, which are the subject of substitution during the binding of the substrates, in the explicit form in the model systems (Scheme 1).

The obtained results (Table 2, entries 4–6) appeared to be coherent with the titration data, *i.e.* the experimentally observed small negative ΔG for the binding of **BH** (approx. −2.5(5) kJ mol^{-1} within 3 st. dev. based on $K = 2.8(2)$ L mol^{-1} at 298 K) and the absence **AA** binding. Moreover, the theoretical calculations indicated that the binding of the O atom in **BH** to the I atom in **H** is more energetically favorable in MeOH than coordination by the N$^{sp^3}$ atom.

Theoretical study of the catalytic mechanism

To understand the catalytic mechanism of **H** in the studied reaction (**BH** + **AA** → **1** + 2H$_2$O), DFT calculations were performed for the first (and apparently rate-limiting) step. Initial calculations indicated that the direct nucleophilic attack of the N^{sp3} atom in **BH** on the C atom in the carbonyl moiety of **AA** was impossible in the absence of **H**. All attempts to fix on the potential energy surface of the zwitterionic intermediate PhC(=O)NHN$^+$H$_2$C(–O$^-$)MeCH$_2$COMe and the corresponding transition state (**TS**) for a nucleophilic attack were unsuccessful in the absence of bound **H** (the geometry optimization procedure resulted in the collapse of the relevant model structures to the initial reactants). Nevertheless, the zwitterionic intermediate formation is possible then **H** is bound to **AA** (Scheme 2, **a–c**; accordingly to the processes on Scheme 1, an additional four MeOH solvent molecules were taken into account in the explicit form).

For the proton transfer from the N atom to the O atom, the inclusion of one MeOH solvent molecule in the reaction mechanism was realized (**TS2**, **TS3**, and **TS4**).[62] Incorporation of the solvent molecule in the transition state of the rate-limiting reaction step was successfully employed by us in previous theoretical studies.[63] For aprotic solvents, at least in the case of
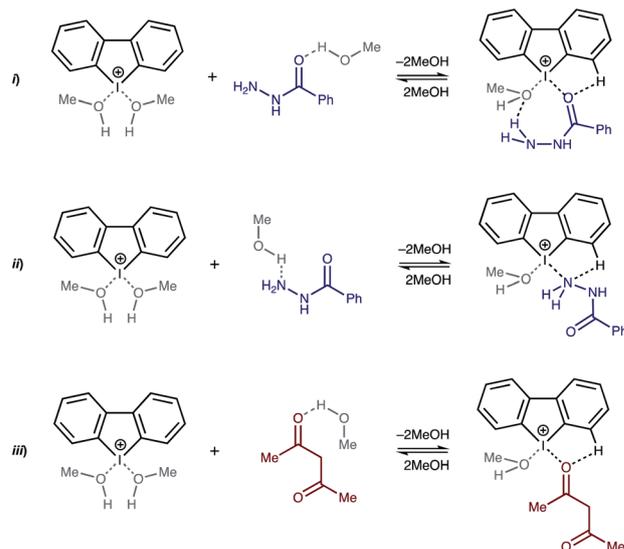
Scheme 1 Model binding reactions.

hydrazine derivatives, an additional molecule of a protic solvent can be changed by a second molecule of the nucleophile.[53]

Next, three reaction paths for the proton transfer were studied, *i.e.*, the catalyzed route provided by the coupling of **H** with **AA** (**C** to **D** *via* **TS2**), the non-catalyzed route (**G** to **E** *via* **TS3**), and the coupling of **H** with the **BH** (**G** to **H** *via* **TS4**). The binding of **H** with an electrophilic substrate (**AA**) resulted in stabilization of the zwitterionic intermediate and reduced the Gibbs free energy of activation for the reaction (Fig. 7, **TS2**). The binding of **H** with **BH** (acting in this reaction as a nucleophile) resulted in a decrease in the energy of the transition state **TS4** in compare with **TS2** and **TS3**, but taking into account that cyclic intermediate **I** was not found, this reaction path was ruled out.

Based on the kinetic measurements, ^{1}H NMR titration data, and DFT calculations, the plausible mechanism of the studied reaction includes the binding of the organocatalyst **H** with **AA** (Scheme 2, a), a nucleophilic attack of the N$^{sp^3}$ atom on the C atom of the carbonyl group of **AA** (b and c), incorporation of a MeOH solvent molecule for the proton transfer (d and e), and regeneration of **H** (f).

To better understand how organocatalyst **H** binds with the reaction substrates, a theoretical estimation of the strength of the hydrogen and halogen bonds in the optimized equilibrium model structures was performed using the topological analysis of the electron density distribution technique (QTAIM analysis, see Table 1S in ESI for details†). The calculations indicated that in all the structures, **H** forms typical noncovalent bonds with ligands and the bond energies of H···O and I···O are 9.2–15.8 kJ mol^{-1} and 19.6–35.7 kJ mol^{-1}, respectively.

Investigation of covalent catalysis by H

Another type of catalysis—through the formation of covalent bonds of the O atom of the **AA** carbonyl moiety—was also checked theoretically. All attempts to fix on the potential energy surface of the different kinds of minima for the Meisenheimer complex-like intermediates were unsuccessful (Fig. 8). Thus,
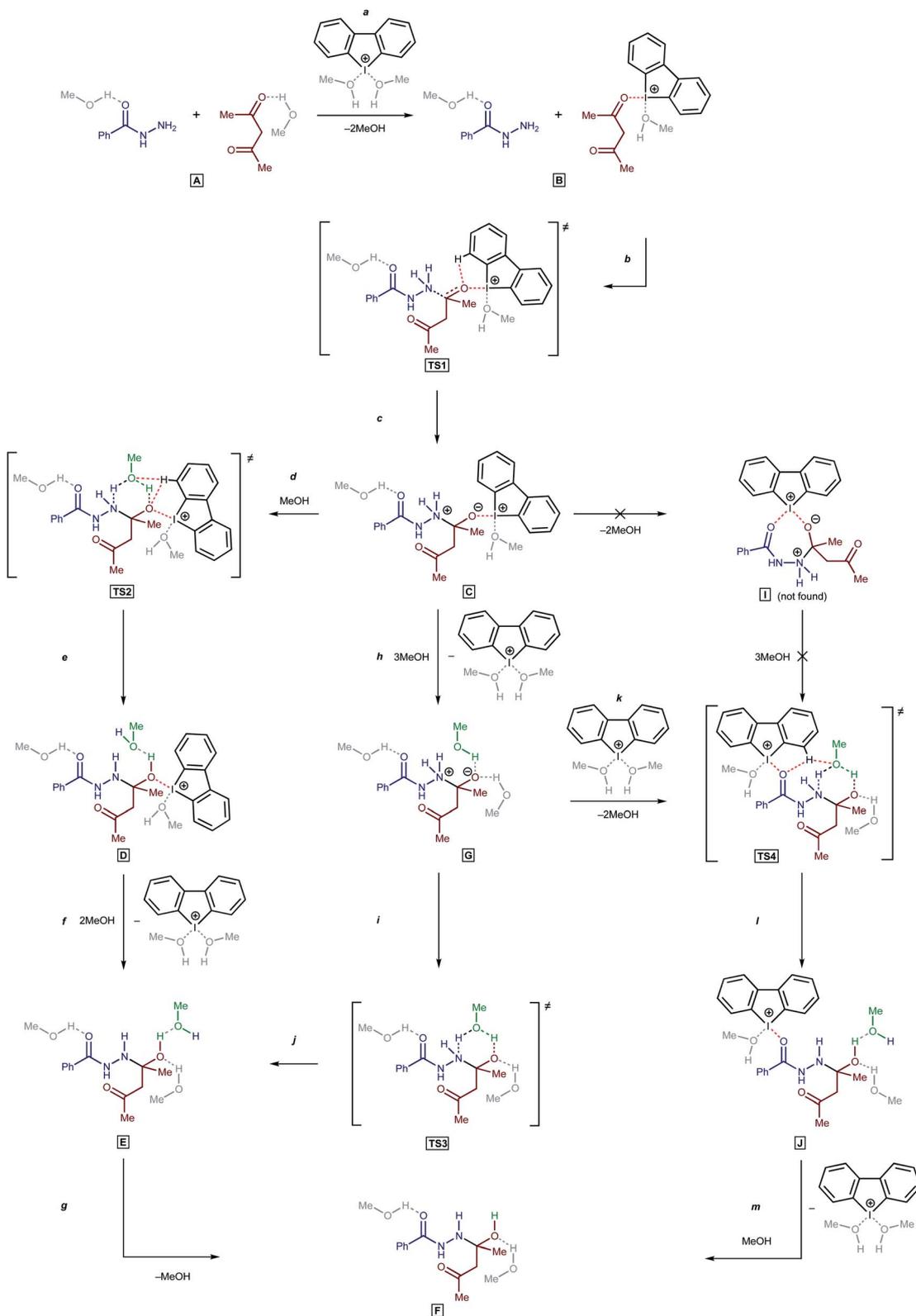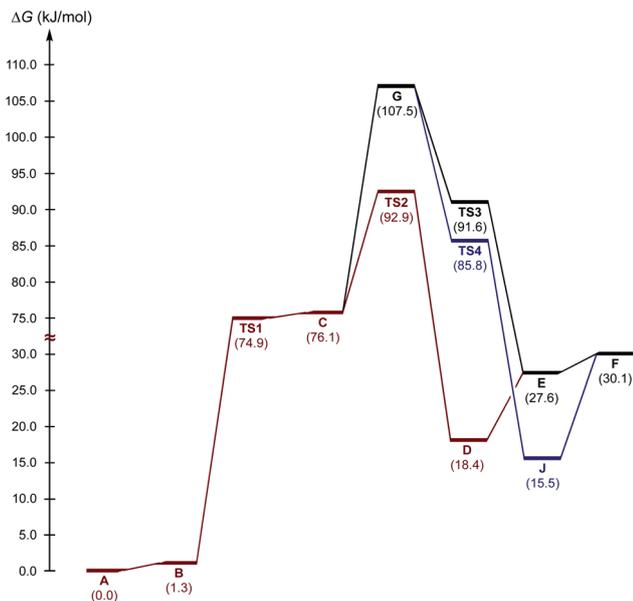
Scheme 2 Possible reaction paths.

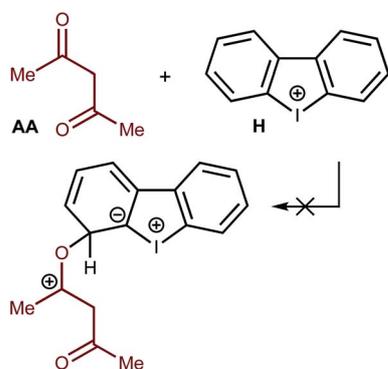Fig. 7 The energy profile for the studied reaction paths.

Fig. 8 One of the five hypothetical Meisenheimer complex-like intermediate.

geometry optimization for the appropriate model species obtained through the formation of O–C–I, O–C–H1, O–C–H2, O–C–H3, and O–C–H4 (accordingly to the numeration on Fig. 4) led to the initial reactants, and these hypothetical structures were excluded from consideration. These results excluded the possibility of covalent catalysis.
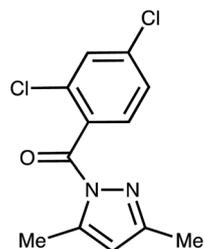
Reaction scope

Dibenzidolium triflate catalyzes the generation of *N*-acyl pyrazoles from **AA** and a series of aromatic and aliphatic acyl hydrazides (Scheme 3). For the aromatic acyl hydrazides, the reaction typically proceeded for 3.5 h, but for the substrates featuring strong EWG NO_2 functionality (**5**) or bulky R_s in the *ortho*-position (**6**, **7**, **10**) heating for 6 h was required. The reaction with the aliphatic acyl hydrazides also required a prolonged reaction time (**12–15**). In all studied cases, the reactions initially were monitored by ^{1}H NMR and each reaction was stopped when the concentration of **1–15** was maximal, rather
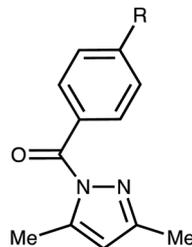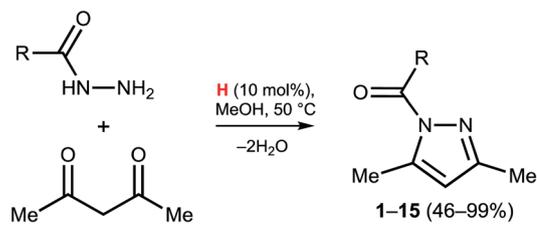
1, R = H, 99% (3.5 h)
2, R = OEt, 95% (3.5 h)
3, R = Me, 99% (3.5 h)
4, R = Cl, 84% (3.5 h)
5, R = NO₂, 46% (6 h)
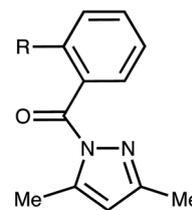
6, R = NH₂, 67% (6 h)
7, R = 1-pyrrolyl, 74% (6 h)
8, R = Me, 90% (3.5 h)
9, R = Cl, 70% (3.5 h)
10, R = CF₃, 75% (6 h)

11, 78% (3.5 h)
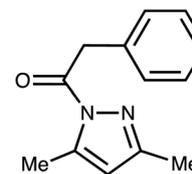
12, 60% (6 h)
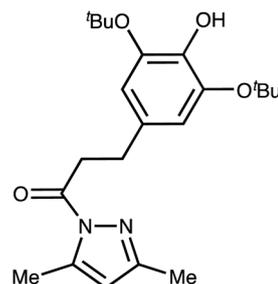
13, 52% (6 h)
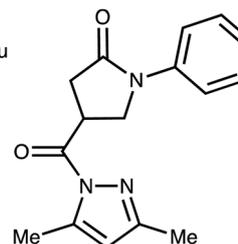
14, 60% (6 h)
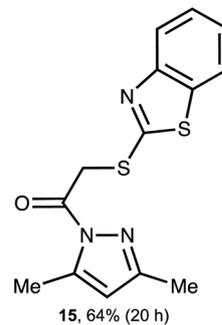
15, 64% (20 h)

Scheme 3 Substrate scope. Isolated yields are given.

than at the maximal conversion. This is caused by the slow solvolysis of **1–15** under the reaction conditions to give 3,5-dimethyl pyrazole and the corresponding RCO_2Me. Our experiments indicated that isolation of the products after 24 h

resulted in reduced yields of the pyrazoles by approximately 25% (except **15**: isolated yield 53% after 24 h).

Conclusions

We found that dibenziodolium salts are convenient iodine(III)-based noncovalent organocatalysts, which effectively catalyze the Knorr-type reactions of *N*-acetyl hydrazides with **AA** to give *N*-acyl pyrazoles. The reactivity of these salts only slightly depends on the identity of the cation, but, as expected,[61] the reactivity of the triflate appears to be higher than the other studied salts. ^{1}H NMR titration data and DFT calculations provided collateral evidence that in MeOH, the catalyst binds to the hydrazide species, which serve as a nucleophile, and this binding proceeds through halogen and hydrogen bonds. Our study indicates that for correct study of binding of iodonium salts with substrates, solvent molecules should be taken into account in the explicit form.

The catalytic effect of the iodonium salt is caused by binding with the ketone, which is less energetically favorable than binding with the hydrazide. Binding to the electrophile results in the reduction of the Gibbs free energy of the transition state of a rate-limiting step of the reaction and thus causes the catalytic effect of the iodonium salt.

Experimental section

Materials and instrumentation

Solvents and acetylacetone were obtained from commercial sources and used as received. Acyl hydrazides[64] and iodine(III) derivatives[65–67] were synthesized by the known methods. All syntheses were conducted in air. Chromatographic separation was carried out on Macherey-Nagel silica gel 60 M (0.063–0.2 mm). Analytical TLC was performed on unmodified Merck ready-to-use plates (TLC silica gel 60 F254) with UV detection. Melting points were measured on a Stuart SMP30 apparatus in capillaries and are not corrected. Electrospray ionization mass-spectra were obtained on a Bruker micrOTOF spectrometer equipped with an electrospray ionization (ESI) source. The instrument was operated in positive ion mode using an m/z range 50–1200. The nebulizer gas flow was 1.0 bar and the drying gas flow 4.0 L min^{-1}. For HRESI$^+$, the studied compounds were dissolved in MeOH. ^{1}H, ^{13}C{^{1}H} and ^{19}F NMR spectra were measured on a Bruker Avance 400 in CD$_3$CN, (CD$_3$)$_2$SO, or CD$_3$OD at 298 K; the residual solvent signal was used as the internal standard.

Preparation procedure for benzoyl hydrazide

A heterogeneous mixture of methyl benzoate (341 mg, 250 mmol) and hydrazine monohydrate (15.0 g, 300 mmol) was refluxed for 18 h during which time a clear colorless solution was obtained. After cooling, all volatile components were evaporated *in vacuo*, and the resulting colorless crystalline solid was dried at room temperature. Recrystallization from benzene/ethanol (5 : 1) gave analytically pure benzohydrazide as colorless needles (27.1 g, 79%).

Preparation procedure for F

2-Iodobiphenyl (0.898 mmol, 251.0 mg) and TFA (1.39 mL) were dissolved in CH$_2$Cl$_2$ (5 mL) and CH$_2$Cl$_2$ was added until a volume of 10 mL was reached. Then the reagent mixture was pumped through an Oxone filled column with a syringe pump (flow rate of 0.11 mL min^{-1}). After the addition of the reagent, the syringe was immediately replaced with a syringe containing CH$_2$Cl$_2$ (10 mL). CH$_2$Cl$_2$ was pumped for 30 min (flow rate of 0.11 mL min^{-1}) and then the flow rate was increased (0.5 mL min^{-1}) until no CH$_2$Cl$_2$ was left in the syringe. The solvent was removed from the resulting solution *in vacuo* and the obtained residue was diluted with water (5 mL). The product was extracted with CH$_2$Cl$_2$ (3 × 5 mL). The organic layer was dried over Na$_2$SO$_4$ and the solvent was removed *in vacuo*. Then Et$_2$O (5 mL) was added to the residue and formation precipitate formation was observed. The suspension was stirred for 10 min and the product was filtered and washed with Et$_2$O (5 mL) and hexane (2 × 5 mL). The product was dried *in vacuo*. Dibenzoiodonium trifluoroacetate **F** (96% yield, 379 mg) was obtained as a beige crystalline solid.

Preparation procedure for G

m-CPBA (77%, 0.736 g, 3.2 mmol) and a solution of HNTf$_2$ (1.26 g, 4.5 mmol) in CH$_2$Cl$_2$ (5.0 mL) were added to a stirred solution of 2-iodobiphenyl (0.56 g, 0.35 mL, 2.0 mmol) in anhydrous CH$_2$Cl$_2$ (6.0 mL). The solution was stirred for 24 h at room temperature, then the solvent was removed on a rotary evaporator. Et$_2$O (10 mL) was added to the remaining solid. The mixture was stirred for 20 min, then filtered. The obtained solid was washed with Et$_2$O three times and dried *in vacuo* to produce dibenziodolium bis(trifluoromethane)sulfonimide **G** (0.84 g, 75%) as a pale-yellow solid.

Preparation procedure for H

m-CPBA (77%, 0.736 g, 3.2 mol) and triflic acid (0.57 mL, 6.5 mmol) were added to a stirred solution of 2-iodobiphenyl (0.56 g, 0.35 mL, 2.0 mmol) in anhydrous CH$_2$Cl$_2$ (6 mL) and stirred for 1 h at room temperature. Then CH$_2$Cl$_2$ was removed *in vacuo*. Et$_2$O (4 mL) was added to the remaining solid. The mixture was stirred for 20 min and then filtered. The obtained solid was washed with Et$_2$O three times and dried *in vacuo* to provide dibenziodolium trifluoromethanesulfonate **H** (0.781 g, 91%) as a white solid.

Preparation procedure for I

Mixture 1 was obtained by dissolving iodobenzene (0.898 mmol, 183 mg, 100 μL) and TFA (1.39 mL) to in CH$_2$Cl$_2$ to achieve a total volume of 10 mL. Mixture 2 was obtained by dissolving 1,3,5-trimethoxybenzene (1.037 mmol) and TFA (2.92 mL) in CH$_2$Cl$_2$ to achieve a total volume of 11 mL.

Mixture **1** was pumped through an Oxone-filled cartridge using a syringe pump (flow rate of 0.11 mL min^{-1}). After 15.5 min, mixture 2 was added using a second syringe pump (flow rate of 0.11 mL min^{-1}). After the addition of mixture **1**, the syringe was immediately replaced with a syringe containing

CH_2Cl_2 (10 mL) and pumped (flow rate of 0.11 mL min^{-1}) until mixture **2** was completely added. Then the flow rate was increased (0.22 mL min^{-1}) for 5 min, then increased again (0.5 mL min^{-1}) until the syringe was empty. The solvent was removed from the resulting solution *in vacuo* and the residue was diluted with water (5 mL). The product was extracted using CH_2Cl_2 (3×5 mL). The organic layer was dried over Na_2SO_4 and the solvent was removed *in vacuo*. Then diethyl ether (5 mL) was added to the residue and a precipitate was formed, the suspension was stirred for 10 min, then the product was filtered and washed with diethyl ether (5 mL) and hexane (10 mL). The obtained product was dried *in vacuo*.

Preparation procedure for J

Finely-crushed, solid 2-iodobenzoic acid (1.0 mmol) was mixed with powdered Oxone (400 mg, 0.65 mmol) in a round-bottomed flask (50 mL) and stirred without a solvent for 5 min using a magnetic stirrer until a homogeneous reaction mass was formed. Then the reaction mixture was cooled with ice to 5 °C and, under magnetic stirring and pre-cooled H_2SO_4 (5 °C, total 0.8 mL) was added in four portions (0.2 mL) to the center of the reaction mixture. After the addition of each portion, the reaction mass was mechanically shaken to achieve thorough mixing—the color of the resulting mass varied from pale yellow to brown depending on the intensity of mixing. After the addition of H_2SO_4, the reaction was continuously stirred for 30 min at room temperature. The mixture was then cooled to 5 °C, CH_2Cl_2 (4 mL) and 1,3,5-trimethylbenzene (3.0 mmol) were added, and was then continuously stirred at room temperature for 3 h. The reaction mixture was re-cooled to 5 °C and CH_2Cl_2 (5 mL) and a saturated aqueous solution of $NaHCO_3$ were added in small portions until pH 8.0 was reached. The organic layer was separated, and the aqueous layer was extracted with CH_2Cl_2 (5 mL). The organic extracts were combined, dried with Na_2SO_4, the solvent evaporated, and the crystalline product was dried *in vacuo*. Additional purification of products can be performed by crystallization from water.

Syntheses of 1–15

Powder of a benzoyl hydrazide (1.0 mmol) was added to a solution of the iodonium salt (0.1 mmol) in methanol (5 mL) placed in a 10 mL round-bottomed flask, whereupon acetylacetone (1.2 mmol) was added to the mixture. The flask was closed and the obtained homogeneous solution (suspension for **12**) was kept at 50 °C for 3.5 h (for **1–8**), 6 h (for **9–14**), or 20 h (for **15**). For **1–15**, crude product was subjected to column chromatography on silica gel (eluted with hexane : ethyl acetate = 4 : 1, v/v) and after collection of the fracture with the product the solvent was evaporated *in vacuo* at 50 °C. A light yellow oil (**1–4, 6, 8–11,** and **13**) and a colorless crystalline solid (**5, 7, 12, 14,** and **15**) were obtained.

Compounds **1–15** were characterized by HRESI$^+$-MS, IR, ^{1}H and ^{13}C{^{1}H} NMR spectroscopies. *N*-Acyl pyrazoles **1–5**,[54,68–71] **7**,[70] **9**,[54] **14**,[72] and **15** (ref. [73]) were previously reported and the spectra of these species prepared by our procedure fully agree with the previously published spectral data. The ESI† file contains characterization and spectra of the compounds **1–15**.

^{1}H NMR monitoring

Optimization of acetylacetone amount (Fig. 3). Acetylacetone (0.01, 0.012, 0.015 mmol) was added to the solution of acetyl hydrazide (0.01 mmol) in CD_3OD (0.3 mL), placed in an NMR tube, whereupon catalyst (0.001 mmol) in CD_3OD (0.3 mL) were added to this mixture. The NMR tube was closed and the obtained homogeneous solution was kept at 50 °C for 70 min in the NMR spectrometer. In this work the reaction was monitored by measuring ^{1}H NMR spectra every 10 min (for 0.012, 0.015 mmol of acetylacetone) and 5 min (for 0.01 mmol of acetylacetone) (4 scans, repetition time 4 s) following the initial equilibration period of 5 min. The reaction was monitored by measuring the time-dependent integral intensity of the CH_3 group signal for product of reaction (**1**).

Optimization of the catalyst amount (Fig. 4). Acetylacetone (0.012 mmol) was added to the solution of acetyl hydrazide (0.01 mmol) in CD_3OD (0.3 mL), placed in an NMR tube, whereupon different amounts of **H** (0, 0.001, 0.005, 0.010 mmol) in CD_3OD (0.3 mL) were added to this mixture. The NMR tube was closed and the obtained homogeneous solution was kept at 50 °C for 70–220 min in the NMR spectrometer. In this work the reaction was monitored by measuring ^{1}H NMR spectra every 10 min (4 scans, repetition time 4 s) following the initial equilibration period of 5 min. The reaction was monitored by measuring the time-dependent integral intensity of the CH_3 group signal for the product of reaction (**1**).

The ^{1}H NMR titration of H with benzoyl hydrazide (Fig. 5 and 6). To a series of solutions of **H** (0.023 mmol) in CD_3CN (0.3 mL) placed in an NMR tube a solution of acetyl hydrazide (0, 0.046, 0.069, 0.092, 0.115 mmol) in CD_3CN (0.3 mL) was added. The ^{1}H NMR spectra were measured at 298 K.

Computational details

The full geometry optimization of all model structures in methanol solution was carried out at the DFT level of theory using the M06-2X functional[74] with the help of Gaussian-09 program package.[75] The quasi-relativistic pseudopotential MWB46 (ref. [76]) that described 46 core electrons and appropriate contracted basis set were used for the iodine atom and standard 6-31G* basis sets were used for other atoms. The solvent effects were taken into account using the SMD (Solvation Model based on Density) continuum solvation model suggested by Truhlar and coworkers.[77] No symmetry restrictions have been applied during the geometry optimization procedure. The Hessian matrices were calculated analytically for all optimized model structures to prove the location of correct minimum or saddle point on the potential energy surface (no imaginary frequencies or only one imaginary frequency, respectively) and to estimate the thermodynamic parameters, the latter being calculated at 25 °C. The topological analysis of the electron density distribution (QTAIM analysis)[78] was performed by using the Multiwfn program (version 3.7).[79] The Cartesian atomic coordinates for all

optimized equilibrium model structures are presented in the attached xyz-files.

Conflicts of interest

There are no conflicts to declare.

Acknowledgements

References

1 V. Oliveira, M. Cardoso and L. Forezi, *Catalysts*, 2018, **8**, 605.

2 Y. Qin, L. Zhu and S. Luo, *Chem. Rev.*, 2017, **117**, 9433–9520.

3 T. Chanda and J. C. G. Zhao, *Adv. Synth. Catal.*, 2018, **360**, 2–79.

4 S. Vellalath and D. Romo, *Angew. Chem., Int. Ed.*, 2016, **55**, 13934–13943.

5 L. Klier, F. Tur, P. H. Poulsen and K. A. Jorgensen, *Chem. Soc. Rev.*, 2017, **46**, 1080–1102.

6 D. M. Flanigan, F. Romanov-Michailidis, N. A. White and T. Rovis, *Chem. Rev.*, 2015, **115**, 9307–9387.

7 S. Mondal, S. R. Yetra, S. Mukherjee and A. T. Biju, *Acc. Chem. Res.*, 2019, **52**, 425–436.

8 H. Guo, Y. C. Fan, Z. Sun, Y. Wu and O. Kwon, *Chem. Rev.*, 2018, **118**, 10049–10293.

9 R. Tepper and U. S. Schubert, *Angew. Chem., Int. Ed.*, 2018, **57**, 6004–6016.

10 D. Bulfield and S. M. Huber, *Chem.–Eur. J.*, 2016, **22**, 14434–14450.

11 X. Zhang, J. Ren, S. M. Tan, D. Tan, R. Lee and C.-H. Tan, *Science*, 2019, **363**, 400–404.

12 C. Bolm, A. Bruckmann and M. Pena, *Synlett*, 2008, **2008**, 900–902.

13 S. M. Walter, F. Kniep, E. Herdtweck and S. M. Huber, *Angew. Chem., Int. Ed.*, 2011, **50**, 7187–7191.

14 F. Kniep, S. H. Jungbauer, Q. Zhang, S. M. Walter, S. Schindler, I. Schnapperelle, E. Herdtweck and S. M. Huber, *Angew. Chem., Int. Ed.*, 2013, **52**, 7028–7032.

15 R. L. Sutar and S. M. Huber, *ACS Catal.*, 2019, **9**, 9622–9639.

16 M. Breugst, D. von der Heiden and J. Schmauck, *Synthesis*, 2017, **49**, 3224–3236.

17 C. M. Volla, I. Atodiresei and M. Rueping, *Chem. Rev.*, 2014, **114**, 2390–2431.

18 C. Thomas and B. Bibal, *Green Chem.*, 2014, **16**, 1687–1699.

19 M. N. Grayson and K. N. Houk, *J. Am. Chem. Soc.*, 2016, **138**, 9041–9044.

20 M. Puripat, R. Ramozzi, M. Hatanaka, W. Parasuk, V. Parasuk and K. Morokuma, *J. Org. Chem.*, 2015, **80**, 6959–6967.

21 N. Busschaert, C. Caltagirone, W. Van Rossom and P. A. Gale, *Chem. Rev.*, 2015, **115**, 8038–8155.

22 X. Fang and C. J. Wang, *Chem. Commun.*, 2015, **51**, 1185–1197.

23 O. V. Serdyuk, C. M. Heckel and S. B. Tsogoeva, *Org. Biomol. Chem.*, 2013, **11**, 7051–7071.

24 F. E. Held and S. B. Tsogoeva, *Catal. Sci. Technol.*, 2016, **6**, 645–667.

25 X. Han, H. B. Zhou and C. Dong, *Chem. Rec.*, 2016, **16**, 897–906.

26 B. L. Zhao, J. H. Li and D. M. Du, *Chem. Rec.*, 2017, **17**, 994–1018.

27 D. Parmar, E. Sugiono, S. Raja and M. Rueping, *Chem. Rev.*, 2014, **114**, 9047–9153.

28 T. Akiyama and K. Mori, *Chem. Rev.*, 2015, **115**, 9277–9306.

29 T. James, M. van Gemmeren and B. List, *Chem. Rev.*, 2015, **115**, 9388–9409.

30 J. Merad, C. Lalli, G. Bernadat, J. Maury and G. Masson, *Chem.–Eur. J.*, 2018, **24**, 3925–3943.

31 F. E. Held, D. Grau and S. B. Tsogoeva, *Molecules*, 2015, **20**, 16103–16126.

32 S. Schindler and S. M. Huber, in *Halogen Bonding II*, ed. P. Metrangolo and G. Resnati, Springer, 2015, pp. 167–204.

33 M. Erdelyi, *Chem. Soc. Rev.*, 2012, **41**, 3547–3557.

34 S. Benz, A. I. Poblador-Bahamonde, N. Low-Ders and S. Matile, *Angew. Chem., Int. Ed.*, 2018, **57**, 5408–5412.

35 D. von der Heiden, A. Vanderkooy and M. Erdélyi, *Coord. Chem. Rev.*, 2020, **407**, 213147.

36 L. Vogel, P. Wonner and S. M. Huber, *Angew. Chem., Int. Ed.*, 2019, **58**, 1880–1891.

37 J. Bamberger, F. Ostler and O. G. Mancheno, *ChemCatChem*, 2019, **11**, 5198–5211.

38 G. Cavallo, P. Metrangolo, R. Milani, T. Pilati, A. Priimagi, G. Resnati and G. Terraneo, *Chem. Rev.*, 2016, **116**, 2478–2601.

39 L. Brammer, G. Mínguez Espallargas and S. Libri, *CrystEngComm*, 2008, **10**, 1712–1727.

40 K. Rissanen, *CrystEngComm*, 2008, **10**, 1107–1113.

41 M. A. Kryukova, D. M. Ivanov, M. A. Kinzhalov, A. S. Novikov, A. S. Smirnov, N. A. Bokach and V. Yu Kukushkin, *Chem.–Eur. J.*, 2019, **25**, 13671–13675.

42 T. M. Beale, M. G. Chudzinski, M. G. Sarwar and M. S. Taylor, *Chem. Soc. Rev.*, 2013, **42**, 1667–1680.

43 S. M. Walter, F. Kniep, L. Rout, F. P. Schmidtchen, E. Herdtweck and S. M. Huber, *J. Am. Chem. Soc.*, 2012, **134**, 8507–8512.

44 S. Libri, N. A. Jasim, R. N. Perutz and L. Brammer, *J. Am. Chem. Soc.*, 2008, **130**, 7842–7844.

45 F. Heinen, E. Engelage, C. J. Cramer and S. M. Huber, *J. Am. Chem. Soc.*, 2020, **142**, 8633–8640.

46 F. Heinen, E. Engelage, A. Dreger, R. Weiss and S. M. Huber, *Angew. Chem., Int. Ed.*, 2018, **57**, 3830–3833.

47 R. Haraguchi, T. Nishikawa, A. Kanazawa and S. Aoshima, *Macromolecules*, 2020, **53**, 4185–4192.

48 Y. Zhang, J. Han and Z.-J. Liu, *RSC Adv.*, 2015, **5**, 25485–25488.

49 T. Clark, M. Hennemann, J. S. Murray and P. Politzer, *J. Mol. Model.*, 2007, **13**, 291–296.

50 M. Nozari, A. W. Addison, G. T. Reeves, M. Zeller, J. P. Jasinski, M. Kaur, J. G. Gilbert, C. R. Hamilton, J. M. Popovitch, L. M. Wolf, L. E. Crist and N. Bastida, *J. Heterocycl. Chem.*, 2018, **55**, 1291–1307.

51 M. J. Kim, S. M. Gaube, M. H. R. Beh, C. D. Smith and A. Thompson, *RSC Adv.*, 2019, **9**, 31773–31780.

52 P. G. Cozzi, *Chem. Soc. Rev.*, 2004, **33**, 410–421.

53 V. K. Burianova, D. S. Bolotin, A. S. Mikherdov, A. S. Novikov, P. P. Mokolokolo, A. Roodt, V. P. Boyarskiy, D. Dar'in, M. Krasavin, V. V. Suslonov, A. P. Zhdanov, K. Y. Zhizhin and N. T. Kuznetsov, *New J. Chem.*, 2018, **42**, 8693–8703.

54 G.-P. Yang, X. He, B. Yu and C.-W. Hu, *Appl. Organomet. Chem.*, 2018, **32**, e4532.

55 B. Balandis, G. Ivanauskaite, J. Smirnoviene, K. Kantminiene, D. Matulis, V. Mickevicius and A. Zubriene, *Bioorg. Chem.*, 2020, **97**, 103658.

56 A. Mumtaz, K. Saeed, A. Mahmood, S. Zaib, A. Saeed, J. Pelletier, J. Sevigny and J. Iqbal, *Bioorg. Chem.*, 2020, **101**, 103996.

57 L. A. Baeva, R. M. Nugumanov, R. R. Gataullin and A. A. Fatykhov, *Chem. Heterocycl. Compd.*, 2020, **56**, 548–554.

58 Z. M. Bikbaeva, D. M. Ivanov, A. S. Novikov, I. V. Ananyev, N. A. Bokach and V. Y. Kukushkin, *Inorg. Chem.*, 2017, **56**, 13562–13578.

59 K. E. Riley, J. S. Murray, J. Fanfrlik, J. Rezac, R. J. Sola, M. C. Concha, F. M. Ramos and P. Politzer, *J. Mol. Model.*, 2011, **17**, 3309–3318.

60 C. B. Aakeroy, M. Baldrighi, J. Desper, P. Metrangolo and G. Resnati, *Chem.–Eur. J.*, 2013, **19**, 16240–16247.

61 R. J. Mayer, A. R. Ofial, H. Mayr and C. Y. Legault, *J. Am. Chem. Soc.*, 2020, **142**, 5221–5233.

62 E. Erdtman, E. A. C. Bushnell, J. W. Gauld and L. A. Eriksson, *Comput. Theor. Chem.*, 2011, **963**, 479–489.

63 D. S. Bolotin, V. K. Burianova, A. S. Novikov, M. Y. Demakova, C. Pretorius, P. P. Mokolokolo, A. Roodt, N. A. Bokach, V. V. Suslonov, A. P. Zhdanov, K. Y. Zhizhin, N. T. Kuznetsov and V. Y. Kukushkin, *Organometallics*, 2016, **35**, 3612–3623.

64 M. H. Klingele and S. Brooker, *Eur. J. Org. Chem.*, 2004, **2004**, 3422–3434.

65 P. S. Postnikov, O. A. Guselnikova, M. S. Yusubov, A. Yoshimura, V. N. Nemykin and V. V. Zhdankin, *J. Org. Chem.*, 2015, **80**, 5783–5788.

66 M. S. Yusubov, N. S. Soldatova, P. S. Postnikov, R. R. Valiev, D. Y. Svitich, R. Y. Yusubova, A. Yoshimura, T. Wirth and V. V. Zhdankin, *Eur. J. Org. Chem.*, 2018, **2018**, 640–647.

67 N. S. Soldatova, P. S. Postnikov, M. S. Yusubov and T. Wirth, *Eur. J. Org. Chem.*, 2019, **2019**, 2081–2088.

68 H. D. Mkoyi, S. O. Ojwach, I. A. Guzei and J. Darkwa, *J. Organomet. Chem.*, 2013, **724**, 95–101.

69 J. M. Ovian, C. B. Kelly, V. A. Pistritto and N. E. Leadbeater, *Org. Lett.*, 2017, **19**, 1286–1289.

70 P. A. Channar, S. Afzal, S. A. Ejaz, A. Saeed, F. A. Larik, P. A. Mahesar, J. Lecka, J. Sevigny, M. F. Erben and J. Iqbal, *Eur. J. Med. Chem.*, 2018, **156**, 461–478.

71 H. Sharghi, J. Aboonajmi, M. Mozaffari, M. M. Doroodmand and M. Aberi, *Appl. Organomet. Chem.*, 2017, **32**, e4124.

72 V. Mickevičius and R. Vaickelioniené, *Chem. Heterocycl. Compd.*, 2008, **44**, 170–172.

73 A. Rutavicius, S. Valiulene and Z. Kuodis, *Chem. Heterocycl. Compd.*, 1995, **31**, 629–633.

74 Y. Zhao and D. G. Truhlar, *Theor. Chem. Acc.*, 2007, **120**, 215–241.

75 M. J. Frisch, G. W. Trucks, H. B. Schlegel, G. E. Scuseria, M. A. Robb, J. R. Cheeseman, G. Scalmani, V. Barone, B. Mennucci, G. A. Petersson, H. Nakatsuji, M. Caricato, X. Li, H. P. Hratchian, A. F. Izmaylov, J. Bloino, G. Zheng, J. L. Sonnenberg, M. Hada, M. Ehara, K. Toyota, R. Fukuda, J. Hasegawa, M. Ishida, T. Nakajima, Y. Honda, O. Kitao, H. Nakai, T. Vreven, J. A. Montgomery Jr, J. E. Peralta, F. Ogliaro, M. Bearpark, J. J. Heyd, E. Brothers, K. N. Kudin, V. N. Staroverov, T. Keith, R. Kobayashi, J. Normand, K. Raghavachari, A. Rendell, J. C. Burant, S. S. Iyengar, J. Tomasi, M. Cossi, N. Rega, J. M. Millam, M. Klene, J. E. Knox, J. B. Cross, V. Bakken, C. Adamo, J. Jaramillo, R. Gomperts, R. E. Stratmann, O. Yazyev, A. J. Austin, R. Cammi, C. Pomelli, J. W. Ochterski, R. L. Martin, K. Morokuma, V. G. Zakrzewski, G. A. Voth, P. Salvador, J. J. Dannenberg, S. Dapprich, A. D. Daniels, O. Farkas, J. B. Foresman, J. V. Ortiz, J. Cioslowski and D. J. Fox, *Gaussian 09, Revision C.01*, Gaussian, Inc., Wallingford CT, 2010.

76 A. Bergner, M. Dolg, W. Küchle, H. Stoll and H. Preuß, *Mol. Phys.*, 2006, **80**, 1431–1441.

77 A. V. Marenich, C. J. Cramer and D. G. Truhlar, *J. Phys. Chem. B*, 2009, **113**, 6378–6396.

78 R. F. W. Bader, *Chem. Rev.*, 1991, **91**, 893–928.

79 T. Lu and F. Chen, *J. Comput. Chem.*, 2012, **33**, 580–592.